Title
CLASSICAL ASPECTS OF THE LASER EXCITATION OF A MORSE OSCILLATOR

Author
Gray, S.K.

Publication Date
1982-07-01

Lawrence Berkeley Laboratory
UNIVERSITY OF CALIFORNIA

Materials & Molecular Research Division

Submitted to Chemical Physics

CLASSICAL ASPECTS OF THE LASER EXCITATION OF A MORSE OSCILLATOR

Stephen K. Gray

July 1982

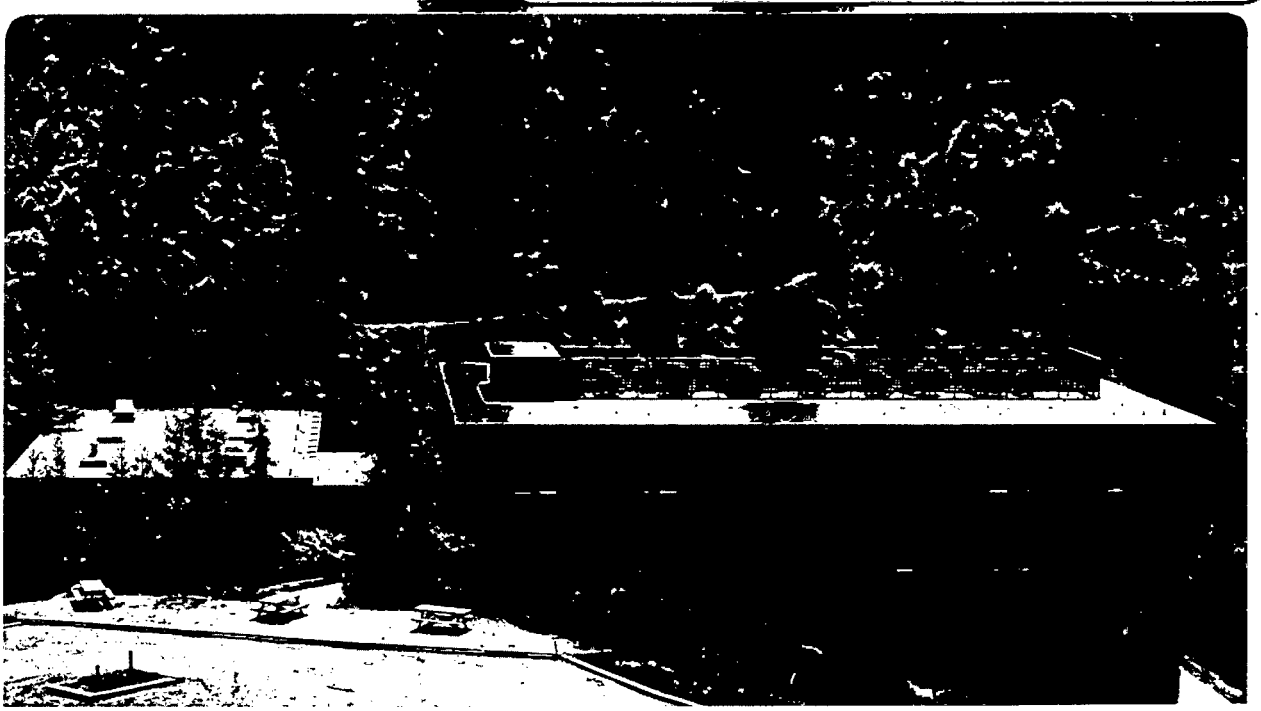

Prepared for the U.S. Department of Energy under Contract DE-AC03-76SF00098

DISCLAIMER

LBL-14717

CLASSICAL ASPECTS OF THE LASER EXCITATION OF A MORSE OSCILLATOR

(Suitable running title: Classical Aspects of Laser Excitation)

Stephen K. Gray

July 1982

Department of Chemistry
Materials and Molecular Research Division
Lawrence Berkeley Laboratory
University of California
Berkeley, CA 94720

This work was supported by the Director, Office of Energy Research, Office of Basic Energy Sciences, Chemical Sciences Division of the U.S. Department of Energy under Contract No. DE-AC03-76SF00098; and in part by the National Science Foundation under Grant CHE-79-20181. Financial assistance from the NSERC of Canada is gratefully acknowledged.

Abstract

A Morse oscillator in an intense laser field is studied classically. A new approach to obtaining the solution, based on construction of a map from initial conditions to the solution after one period of oscillation of the laser, is given. The solution over many periods is then examined by repeatedly applying the map. The solution, as a function of time, is seen to exhibit some very interesting behavior, including spirals or "whorls" in phase space. The pendulum model of nonlinear resonance is shown to describe this behavior reasonably well and, in fact, can be used to crudely interpret dynamical trends, such as the average energy absorption as a function of initial vibrational state.

I. Introduction

With the development of high-powered lasers, physical chemists have been exploring the nature of multiphoton and overtone absorption in molecules[1]. There is a growing need for simple theoretical models to interpret and predict the results of such experiments. However, the correct theoretical treatment, a detailed solution of Schrodinger's equation, is still out of reach for most systems of chemical interest. Many theoreticians have thus turned to a classical description of the process, which is at least more tractable. The justification for using classical mechanics, aside from the tractability, is based on several numerical comparisons of exact quantum and classical solutions for some relatively simple systems[2]. These results suggest that certain averaged quantities, such as the pulse time averaged energy absorption, are described reasonably well with classical mechanics. However, it is important to realize that many specific details of the absorption, such as rotational fine structure, cannot be well described within a classical framework[2c].

Given that a classical description of molecular energy absorption is to some extent correct, there is still a need to understand more clearly the nature of this description. Most classical trajectory studies are essentially numerical experiments, involving the solution of many coupled nonlinear differential equations. There is a need to understand how and why a solution comes out as it does and, moreover, to build more general models of the process that don't require any

detailed numerical calculations.

In this paper, the simplest model of a laser induced process, the excitation of a Morse oscillator in an intense laser, is examined classically in detail. First, a new approach to the solution, based on generating a map that takes initial conditions to the corresponding solution after one period of oscillation of the laser, is presented. Repeated applications of this period advance map[3] then allow the solution over many periods to be obtained with relative ease. The behavior of the solution, as a function of time, or the number of oscillations of the laser, is found to be quite interesting, with spirals or "whorls" developing in phase space. Such behavior has been discussed by Berry and co-workers[4] for simpler maps, and can be related to some elementary properties of the map. We then go on to show that a very simple model, due primarily to Chirikov[5], and based on the orbits of a pendulum, is capable of describing this behavior reasonably well. The pendulum model is found to be a useful tool for understanding other features of the dynamics, such as certain trends in the average energy absorption as a function of initial vibrational state.

In sec. II, the period advance map and its generation are discussed. Sec. III applies the method to a nonrotating HF molecule in an intense laser field. Sec. IV uses the pendulum model to interpret the results of sec. III, and sec. V discusses energy absorption trends qualitatively with the pendulum model. Finally, sec. VI consists of some brief concluding remarks.

II. The Period Advance Map

Consider a one-dimensional nonlinear oscillator, driven by a periodic force $f(x,t) = f(x,t + \tau)$. The Hamiltonian is written

$$H(p,x,t) = p^2/2\mu + V(x) + f(x,t) \quad , \tag{2.1}$$

where p and x are the canonically conjugate momentum and position, μ is the mass, and $V(x)$ is the unperturbed potential function. Hamilton's equations are periodic in time and read

$$\begin{aligned} \dot{p}(t) &= -\partial H/\partial x = \dot{p}(t + \tau) \\ \dot{x}(t) &= \partial H/\partial p = \dot{x}(t + \tau). \end{aligned} \tag{2.2}$$

In many applications, such as those in Ref. 2, the periodicity of eqs. (2.2) is not used as a practical simplification. Rather, a direct numerical integration, for each trajectory in a given ensemble, is performed over many periods τ of the driving force. If eqs. (2.2) were linear, however, Floquet analysis[6,7] does allow one to make effective use of the periodicity. Moreover, in the quantum analogue of the problem, because the differential equations for the coefficients of the wavefunction are always linear, even when the corresponding classical equations are nonlinear, the periodicity again simplifies the calculations[2a,7]. It was the apparent lack of a practical scheme, making use of the periodicity of the nonlinear classical equations, that was the

original motivation for this work.

The approach taken here is based on the period advance map[3]; which maps initial conditions (p_o,x_o) to the corresponding solution at $t = \tau$, (p_τ,x_τ) :

$$(p_\tau,x_\tau) = T(p_o,x_o) \quad . \tag{2.3}$$

An elementary property of the periodicity of eqs. (2.2) is that once the solution over the first period is known, then it is known for all subsequent period advances by repeatedly applying the map :

$$(p_{r\tau},x_{r\tau}) = T^r(p_o,x_o),\ r = 1,2,3,... \tag{2.4}$$

In addition to the useful and practical property (2.4), it is a straightforward consequence of Liouville's theorem that T is an area preserving map[3].

A functional representation of eq. (2.3) is

$$\begin{aligned} T_p(p_o,x_o) &= p_\tau \\ T_x(p_o,x_o) &= x_\tau \end{aligned} \quad , \tag{2.5}$$

where T_p and T_x are two-dimensional functions spanning the relevant phase space. To obtain approximations to T_p and T_x, one may simply define a grid of initial conditions (p_o^i,x_o^j) and for each grid point (i,j)

numerically integrate over one period of the motion to obtain T_p^{ij} and T_x^{ij}. Any appropriate two-dimensional fitting function may be used to define the approximations to T_p and T_x. Of course to obtain accurate approximations, a dense grid of initial points, such as a 100 x 100 grid, must be used. However, the numerical integration of even a very dense grid over only one period of the driving force is usually a very quick and easy task. Furthermore, once T has been satisfactorily determined, the solution over many periods of oscillation is known from eq. (2.4).

In the calculations reported below, use was made of two-dimensional cubic spline functions to define T_p and T_x. The advantage of using splines is that they pass uniquely through all the data points, and can be shown to have desirable minimum curvature properties[8a]. A cubic spline is a piecewise continuous interpolating polyanomial with continuous first and second derivatives. A possible disadvantage of using splines is then that higher order derivatives may not be continuous. However, no problems were encountered in the present application. The explicit algorithm used here is that of Ref.8b, with the one-dimensional splines required by this algorithm chosen to be the natural cubic splines of Ref.8a.

III. Application to a Diatomic in an Intense Laser

A. Action-Angle Variables

Frequent use will be made of the Morse oscillator action-angle variables, so it is convenient to define them here. The Hamiltonian for a Morse oscillator, in the absence of any driving force, is

$$H_o(p,x) = p^2/2\mu + D(e^{-\alpha x}-1)^2 \quad , \tag{3.1}$$

where D is the dissociation energy, and α is a positive constant related to the curvature of the potential. For convenience, x has been taken to be the displacement from equilibrium. It is possible to change variables from (p,x) to action-angle variables (n,q) such that $H_o = H_o(n)$, i.e. the new Hamiltonian is a function of the action n only. Rankin and Miller[9] have done this for the Morse oscillator, with the result

$$H_o(n) = (n + \hbar/2)\omega_o - (n + \hbar/2)^2\omega_o^2/4D \quad , \tag{3.2}$$

where $\omega_o = \sqrt{2D\alpha^2/\mu}$. The unperturbed motion is then given by $\dot{n} = 0$, and $\dot{q} = \omega(n)$, where the oscillator frequency is

$$\omega(n) = \partial H_o/\partial n = \omega_o - (n + \hbar/2)\omega_o^2/2D \quad . \tag{3.3}$$

The old variables (p,x) are related to the new variables (n,q) by

$$\left.\begin{aligned} x(n,q) &= \alpha^{-1} \ln[\,(D + \sqrt{DH_o(n)}\,\cos q)/(D - H_o(n))] \\ p(n,q) &= \mu\omega(n)\partial x/\partial q \\ &= -\mu\alpha^{-1}[\,\omega_o - (n + \hbar/2)\omega_o^2/2D\,]\,\frac{\sqrt{DH_o}\,\sin q}{(D + \sqrt{DH_o}\,\cos q)} \end{aligned}\right\} \qquad (3.4)$$

The phase convention in eqs. (3.4) has been chosen so that $q = 0$ is an outer turning point and $q = \pi$ is an inner turning point.

It should be noted that n corresponds closely with the vibrational quantum number v. Thus if one replaces n with $v\hbar$, $v = 0,1,\ldots$, eq. (3.2) gives the correct energy eigenvalue formula for the Morse oscillator. We use atomic units ($\hbar = 1$) throughout, so that classically n can take on any value $\geq -1/2$ and $0 \leq q \leq 2\pi$.

B. Generating the Period Advance Map

To mimic a nonrotating HF molecule in a strong laser, a Morse potential was used with a driving force linear in x (i.e. the linear dipole approximation),

$$H(p,x,t) = p^2/2\mu + D(\,e^{-\alpha x} - 1\,)^2 - \varepsilon x \cos\Omega t, \qquad (3.5)$$

with $\varepsilon = \sqrt{8\pi I/c}\,d_1$, where I is the laser intensity, c the speed of light, and d_1 the slope of the dipole. For HF, one has[2a] $D = 0.25509$, $\alpha = 1.1741$ and $\mu = 1744.8$ a.u. With[7b] $d_1 = 0.3099$ a.u., $\varepsilon = 0.00165$ a.u. for a 1 TW/cm^2 laser intensity. The laser frequency was taken to be the fundamental transiton frequency, i.e. $\Omega = H_o(1) - H_o(0) = 0.01807$ a.u. The period is then $\tau = 2\pi/\Omega = 347.7$ a.u. (or 0.00841 ps).

The period advance map was then obtained by the method described in sec. II. A suitable grid for the present purposes was a 100 x 100 grid with x_o and p_o evenly spaced between $-0.3573 \leq x_o \leq 0.6274$ and $-14.61 \leq p_o \leq 14.61$. These limiting values allow for excitations up to $n = 3$. As a check on the accuracy of the map so obtained, comparsion was made with trajectories that were directly integrated over r periods of the driving force. In Table I is shown the root mean square deviations of the predicted $p_{r\tau}, x_{r\tau}$ values from the map and the directly integrated trajectories for an ensemble of 50 trajectories with $n = 0$ initially and q evenly spaced between 0 and 2π. The map is seen to be accurate over the first few hundred periods. However, the numerical interpolation error builds up, particularly in $p_{r\tau}$, as r increases, and the map cannot be expected to be very accurate beyond $r \sim 400$. This error could be improved, of course, if a finer grid, particularly in p_o, were used, but the present form is sufficient for our purposes.

It should be noted that although it was necessary to integrate numerically 10,000 trajectories over one period of the driving force, the resulting map contains information that would be much more difficult to obtain by direct integrations over many periods of oscillation. For example, the behavior of the entire phase plane will be examined below with the map.

C. Repeated Iterations of the Map

If one takes some initial set of (p,x) points and repeatedly maps them, plotting each mapped point, one obtains the surface of section plot shown in Fig. 1a. Points on each curve labeled A through E will, upon successive mappings (or periods of oscillation), yield points on the same curve. Thus, for example, if one starts with some point on curve C, it will, upon repeated mappings, travel counterclockwise around C in uneven but discrete jumps. The period 1 fixed points, i.e. those points satisfying (p,x) = T(p,x), lie, by the symmetry of the underlying Hamiltonian, on the x axis. These points are classified as being stable elliptic (o in Fig. 1) or unstable hyperbolic(•) fixed points depending on whether mapped points, in a small region about each fixed point, fall on closed ellipses or open hyperbolas. The elliptic or hyperbolic nature of each fixed point was also verified by a linearization of the map about each fixed point[10]. With T defined in terms of the cubic splines, the required derivatives could be obtained analytically.

As a check on the accuracy of the map, the fixed points were also found by direct integrations of trajectories and agreed, to six significant figures, with the map predictions. Incidentally, there is one more fixed point, that lies at $x = \infty$, so that the total number of fixed points is even, as would be expected[10]. There are also higher order fixed points, $(p,x) = T^s(p,x)$, $s > 1$, which will be mentioned later on.

Also, the approximate positions of the period 1 fixed points can be predicted remarkably well with some simple arguments given in the Appendix.

It may appear, from Fig. 1a , that the motion is quite complicated. However, if one plots the curves in action-angle space, with n and q as defined previously, one obtains Fig.1b. The curves in (n,q) space bear a close resemblance to orbits of a simple pendulum[5,11] . In fact, this analogy will be made more clear in sec.IV. By symmetry, the three relevant fixed points now lie at either $q = 0$ or $q = \pi$. The two most important of these points are $(n,q) = (0.61726, \pi)$, which is stable, and (0.36030, 0), which is unstable. Notice that these points have action values near $n = 1/2$, which is the action where the molecular frequency is in resonance with the laser frequency ($\omega(1/2) = \Omega$). The other fixed point, which lies at (-0.48206, 0), and is stable, corresponds to the molecule having practically no energy. Some orbits, very near this point, must close around it. However, this occurs only in a very small region and most orbits , even for n values as small as -0.4, appear as "rotations" (e.g. curve E in Fig.1b). We will not concern ourselves with the region very close to this point.

As a final point on the surface of section plots, no "chaotic" regions were noticable with the present perturbation strength ϵ. Of course these regions do exist,[5] particularly near the separatrix curves B and D, which are the sets of points which eminate from and approach the unstable fixed point, but are small in area and difficult to see on the scale of the plots.

It is of interest to see how a line in action-angle space, which corresponds to an initial classical vibrational state, behaves under the mapping. In Fig. 2 is shown the result of mapping points that lie initially on a line in (n,q) space with $n_o = 1/2$ and q_o between 0 and 2π. It is seen that the line distorts into quite a remarkable structure. Spirals or whorls develop near the stable fixed point (o). Although not shown here, even more applications of the map results in the whorls winding more and more about the stable fixed point. The behavior near the unstable fixed point (•) is also interesting. Initially no point lies on the unstable fixed point, but very quickly under the mapping points begin to approach it closely. Fig. 3 shows the results of mapping points that lie initially on lines with $n_o = 0$ and 1. The behavior of these initial states is similar to $n_o = 1/2$, with, for example, whorls again evolving about the stable fixed point.

Berry and co-workers[4] have considered the fate of curves under mappings. They expect to see whorls near stable fixed points, which indeed are observed here. In the next section, this behavior will be seen to also arise out of the pendulum analogy[5]. Berry and co-workers[4] also predict "tendrils", or chaotic and snake-like convolutions, to develop near the unstable fixed point. Tendrils are not observed here. The reason that the tendrils are hard to see is that they are associated with the chaotic motion near the separatrix. As we have already noted, this region is quite small here, so that tendrils are not evident on the scale of Figs. 2 and 3. However,

if one expanded the scale, and looked very carefully, tendrils may be evident.

Another interesting manifestation of the whorls is evident in a coarse-grained glance at the entire phase plane evolving under the map. Consider dividing the initial phase space into, say, a 120 x 120 grid of points with $-1/2 \leq n_o \leq 5/2$, and $0 \leq q \leq 2\pi$. Each point of this grid is then mapped and the resulting new action at time $r\tau$, $n_{r\tau}(n_o,q_o)$, is plotted in a coarse-grained fashion. If $n_{r\tau}$ is between -1/2 and 1/2, corresponding to a crude n = 0 state, white coloring is used. If $n_{r\tau}$ is between 1/2 and 3/2, corresponding to an n = 1 state, grey coloring is used. If $n_{r\tau}$ is between 3/2 and 5/2, an n = 2 state, diagonal lines are used. Finally, if $n_{r\tau}$ is between 5/2 and 7/2, an n = 3 state, dots are used. At time zero (i.e. r = 0), one has simply rectangular blocks with white on bottom, grey on top of the white, and diagonal lines on top of the grey. After 20 periods of oscillation of the laser, one obtains Fig. 4a , which shows a developing whorl in the n = 1/2 resonance region. Notice that the axes in Fig. 4 are always the initial action and angle variables, and the coloring represents the coarse-grained action at time $r\tau$ that evolved from those initial conditions. After 40 and 60 oscillations one obtains Figs. 4b and 4c, with the whorl winding more tightly in the resonance region. Although not shown here, this has been followed for up to 400 periods of the driving force, with the whorls winding tighter and tighter, representing very graphically how molecules absorb and emit

energy in the vicinity of a resonance.

IV. The Pendulum Model

The remarkable similarity of the surface of section plot Fig. 1b and the pendulum phase plane orbits[5,11] can be made more concrete. In fact, Chirikov[5] has developed a theory of classical resonance based on this analogy. Here, similar ideas are applied to the forced Morse oscillator problem of sec. III.

A. Derivation of the Pendulum Hamiltonian

In action-angle variables, the full Hamiltonian is

$$H(n,q,t) = H_o(n) - \epsilon x(n,q) \cos\Omega t \quad . \tag{4.1}$$

In our problem, $x(n,q)$, defined by eq. (3.4), is an even function of q so that the perturbation may be expanded in a cosine Fourier series with the result

$$x(n,q) \cos\Omega t = \Sigma_{k=o}^{\infty} V_k(n) \left[\cos(kq - \Omega t) + \cos(kq + \Omega t) \right] , \tag{4.2}$$

where

$$V_k(n) = (2\pi)^{-1} \int_{-\pi}^{\pi} dq \; x(n,q) \cos kq \quad . \tag{4.3a}$$

The integral of eq. (4.3a) may be evaluated analytically[12] for x(n,q) given by eq. (3.4) ,to yield explicit expressions for the Fourier coefficients,

$$V_k(n) = - d^{-k}/\alpha k \quad , \; k \neq 0$$
$$V_o(n) = \alpha^{-1} \ln \left(- \sqrt{H_o/D}\, d/2 \right) \quad , \qquad (4.3b)$$

where $d = - \sqrt{D/H_o} \left(1 + \sqrt{1 - H_o/D} \right)$.

Now the important terms in the expansion of eq. (4.2) are those with slowly varying arguments. If one is looking at a region of phase space with the action n near n_1, the primary resonance defined by

$$\omega(n_1) - \Omega = 0 \quad , \qquad (4.4)$$

where $\omega(n)$ is the oscillator frequency given by eq. (3.3), then the term $q - \Omega t$ is slowly varying, since $\dot{q} - \Omega \approx \omega(n_1) - \Omega = 0$. Thus one may keep only the relevant (k=1 is eq. (4.2)) term in the Fourier expansion, which results in the approximate Hamiltonian, valid near $n = n_1$, of

$$H(n,q,t) \approx H_o(n) - \varepsilon V_1(n) \cos(q - \Omega t) \quad , \qquad (4.5)$$

where the $\cos(q + \Omega t)$ term has also been assumed very oscillatory and neglected. Next, one transforms to a new angle variable $\hat{q} = q - \Omega t$, which corresponds to the difference between molecular and laser phases. This may be accomplished with a generator [5,11] $F_3(n,\hat{q},t) = -(n-n_1)(\hat{q}+\Omega t)$, which implicitly defines the new variables $\hat{p}$ and $\hat{q}$ through $\hat{n} = -\partial F_3/\partial\hat{q}$ and $q = -\partial F_3/\partial n$. This results in $\hat{p} = n-n_1$, $\hat{q} = q - \Omega t$, and the new Hamiltonian

$$\begin{aligned} K &= H(\hat{p},\hat{q},t) + \partial F_3/\partial t \\ &= H_o(\hat{p} + n_1) - \varepsilon V_1(\hat{p} + n_1)\cos\hat{q} - \hat{p}\Omega \quad . \end{aligned} \tag{4.6}$$

The final step is to expand H_o about $\hat{p} = 0$ (i.e. $n = n_1$) to quadratic order and V_1 to zero order. Since H_o is already quadratic in n (see eq. (3.2)), the expansion of H_o is exact here. The result is

$$K - H_o(n_1) = \hat{p}^2/2M_1 - \varepsilon V_1(n_1)\cos\hat{q} \quad , \tag{4.7}$$

where $M_1^{-1} = (\partial\omega/\partial n)_{n_1}$. Eq. (4.7) is the Hamiltonian for a pendulum of mass M_1, which for the Morse oscillator, from eq. (3.3), is

$$M_1 = -2D/\omega_o^2 < 0 \quad .$$

To make the connection with the more familiar positive mass pendulum orbits, one may note that the equations of motion consistent with eq. (4.7),

$$\dot{\hat{p}} = -\partial K/\partial \hat{q} = -\varepsilon V_1(n_1)\ \sin\hat{q}$$
$$\dot{\hat{q}} = \partial K/\partial \hat{p} = \hat{p}/M_1 \quad ,$$

are the same as

$$\dot{\hat{p}} = \varepsilon V_1(n_1)\ \sin\hat{\theta}$$
$$\dot{\hat{\theta}} = \hat{p}/m_1 \quad , \qquad (4.8)$$

with $\hat{\theta} = -\hat{q}$ and $m_1 = -M_1 > 0$. But eqs.(4.8) are consistent with the Hamiltonian

$$K' = \hat{p}^2/2m_1 + \varepsilon V_1(n_1)\ \cos\hat{\theta} \quad , \qquad (4.9)$$

where $(\hat{p},\hat{\theta})$ are the conjugate variables. Thus the well known pendulum orbits $\hat{p}(t),\hat{\theta}(t)$ will determine the approximate motion of a forced Morse oscillator when the action is close to n_1 through $n(t) = \hat{p}(t) + n_1$, and $q(t) = \Omega t - \hat{\theta}(t)$.

The separatrix associated with eq.(4.9) will have maximum and minimum values of action for $\hat{\theta} = \pi$ and $K' = \varepsilon V_1$, if $V_1 > 0$. If $V_1 < 0$, then they occur for $\hat{\theta} = 0$. In either case, the maximum and minimum separatrix actions may be obtained, in terms of the original Morse action variable, from

$$n_1^{\pm} = n_1 \pm 2\sqrt{\varepsilon |V_1| m_1} \quad . \qquad (4.10)$$

A similar analysis may be made about other resonances. For example, the next resonance corresponds to an "overtone" resonance, $2\omega(n_2) - \Omega = 0$. In this region of action space, $2q - \Omega t$ is slowly varying so that the k=2 Fourier term in eq. (4.2) may be singled out. The same analysis as above, but with a classical generator of the form $F_3(n,\hat{q},t) = -(n-n_2)(\hat{q} + \Omega t)/2$, yields

$$K_2' = \hat{p}^2/2m_2 + \varepsilon V_2(n_2) \cos\hat{\theta} \quad ,$$

where now $\hat{p} = (n-n_2)/2$, $\hat{\theta} = \Omega t - 2q$, and $m_2^{-1} = 4\left|\partial\omega/\partial n\right|_{n_2}$. The fixed points associated with the n_2 resonance are actually period 2 fixed points of the period advance map. The maximum and minimum separatrix action values, in the original Morse action, are

$$n_2^{\pm} = n_2 \pm 4\sqrt{\varepsilon|V_2|m_2} \quad . \tag{4.11}$$

In order for the pendulum model to be valid, the neglected terms in the Fourier expansion must indeed be rapidly oscillating compared to the terms kept. Chirikov[5] has shown that a condition for this to be so is the condition of moderate nonlinearity,

$$\varepsilon \ll \alpha_r = \left|\partial\omega/\partial n\right| \omega/n \ll 1/\varepsilon \quad . \tag{4.12}$$

It is also necessary that the separatrices associated with, say, the primary resonance n_1 and the next resonance n_2, do not overlap much -

i.e. are well separated from each other. Chirikov[5] defines the coupling constant of the resonances, s, such that if

$$s = \Delta\omega/\Delta \ll 1 \quad , \tag{4.13}$$

then the relevant resonances are sufficiently separated from one another. In eq. (4.13), $\Delta\omega$ could be the frequency full width of the separatrix of the primary resonance, $\Delta\omega = |\partial\omega/\partial n|\ (n_1^+ - n_1^-) = 4\sqrt{\varepsilon|V_1|/m_1}$, and Δ, the difference between the primary resonance frequency $\omega(n_1)$ and the next resonance frequency $\omega(n_2)$. If $s \gtrsim 1$, then the overlap of resonances is associated with chaotic behavior in the vicinity of the separatrices[5].

B. Pendulum Approximation to Nonrotating HF in a Strong Laser

For the problem of sec. III, it is readily found that $n_1 = 1/2$, $m_1 = 1266$, and $\varepsilon V_1(n_1) \simeq 2.04 \times 10^{-4}$, using the formulae given above. The moderate nonlinearity condition, eq. (4.12), is also found to be satisfied, since then $\varepsilon \sim 0.002$, and near $n_1 = 1/2$, $\alpha_r \sim 0.02$. The resonance coupling constant s also satisfies eq. (4.13), since the next resonance is $n_2 \simeq 12$, and is thus well separated from n_1 ($s \lesssim 10^{-1}$).

From the above considerations, one expects that the pendulum model will be reasonably adequate. Indeed, if one uses eq. (4.10) to estimate the maximum and minimum separatrix action values, one finds $n_1^+ = 1.5$ and $n_1^- = -0.5$, in reasonable agreement with the actual values, which from Fig. 1b are closer to 1.6 and -0.35.

The fixed points of the pendulum described by eq.(4.9), when converted back to the original action-angle variables, occur at $(n,q) = (1/2, \pi)$ and $(1/2,0)$, and are stable and unstable respectively. These fixed points agree reasonably well with the two most important fixed points of the problem discussed in sec.IIIC . The pendulum model does not have the additional fixed point, near $n = -1/2$, that occurs in the full problem. However, the immdeiate region near this point is of no concern to us here, and, furthermore, the pendulum orbits do actually describe the motion near (but not very near) this point reasonably well, as might be guessed from inspection of Fig.1b.

The pendulum equations of motion, eqs.(4.8), were solved numerically, since although analytical solutions do exist, in terms of elliptic integrals[5,6], they are somewhat cumbersome to use. Fig. 5 shows the result of following the behavior of classical states with $n_o = 1/2$, 0 and 1, just as was done in sec.IIIC. By comparison with Figs. 2 and 3 for the full problem, it is seen that the major qualitative features of the dynamics, including the whorls, arise out of the pendulum equations of motion. It will also be noticed from Fig.5 that there is an artifact in the pendulum solution in that the action is now no longer bounded from below. Thus some points actually map to below $n = -1/2$, which is nonphysical since n for the Morse oscillator is only defined for $n \gtrsim -1/2$.

Tendrils are absent entirely, even under very close scrutiny, because no chaotic trajectories exist in the pendulum phase space. The fact that they are also difficult to see in the full problem is

related to the smallness of the resonance coupling parameter s.

It is also easy to see why points, initially not on or extremely close to the unstable fixed point will eventually approach it closely. If one starts with an initial line in (n,q) space, which is also a line in the pendulum phase space $(\hat{p},\hat{\theta})$, then as long as $\hat{p} = n - n_1$ is within the width of the separatrix, the line must intersect the separatrix twice. Points on the separatrix will tend to move towards an unstable fixed point, or, equivalently, away from another unstable fixed point (cf. curves B and D in Fig. 1b), but never actually reach the unstable fixed point in finite time. Thus, since all the values of n_o studied are within the separatrix width, necessarily points intersect the separatrix and then approach the unstable fixed point.

The origin of the whorls can be seen in terms of the nonlinearity of the pendulum equations of motion. Because each orbit about the stable fixed point has a different frequency, or rotation number[4,10], a line that intersects these orbits will then wind about the fixed point, with different points winding faster than other points, thus forming a whorl.

V. Energy Absorption Trends

In this section, the pendulum model of sec.IV is used to predict qualitative trends in the average energy absorption[13] of Morse oscillators initially in different vibrational states. Suppose, for

example, one has an initial classical state with n_o fixed and q_o evenly distributed between 0 and 2π. This corresponds to a horrizontal line across Fig. 1b. Now each point on the line will evolve, following the pendulum-like surface of section lines in the figure. Rather than follow this motion explictly, either by the period advance map, or by direct integration of trajectories, one can use the pendulum model to predict in advance whether there will be a net gain or loss of energy. Suppose n_o lies between the minimum separatrix action n_1^- and the primary resonance action n_1. Then a substantial number of points on the initial line will follow elliptic closed orbits about n_1. But these points then spend most of their time above n_o, since $n_o < n_1$, which results in a net gain of energy (recall n is a measure of the energy - eq.(3.2)). Conversely, if n_o lies between n_1 and n_1^+, the maximum in the primary separatrix action, then again the points will orbit about n_1, but spend most of their time below n_o, resulting in a net energy loss. If n_o is outside the separatrices, then the points will simply rotate up and down (as in curve A of Fig.1b) , , and, other things being equal, will not gain or lose much energy. However, if n_o is increased to within the separatrix corresponding to the next resonance, i.e. the overtone resonance n_2, there will again be a net energy gain if n_o is between n_2^- and n_2, and a net energy loss if n_o is between n_2 and n_2^+.

Recently, Christoffel and Bowman[13] have looked at the net energy absorption of nonrotating HF molecules as a function of initial

vibrational action using classical trajectories. They used a larger perturbation strength than that of secs. III and IV, $\varepsilon \simeq 0.011$, and a slightly different laser frequency, $\Omega = 0.01787$ a.u. The primary resonance is found from eq.(4.4) to be $n_1 = 0.752$. From eq.(4.10), the minimum and maximum separatrix actions are $n_1^- = -2.0$ and $n_1^+ = 3.5$. An action of -2 is nonphysical, but is irrelevant for the arguments that follow. Similarly, the overtone resonance is found from $2\omega(n_2) - \Omega \mp 0$, and is $n_2 = 12.06$. From eq.(4.11) the associated action extrema are $n_2^- = 9.1$ and $n_2^+ = 15.0$. Rounding off crudely, one would expect initial actions n_o between 0 and 1 to have a net energy gain, 1 and 4 to have a net energy loss, 4 and 9 to neither gain nor lose much energy, and once again increased absorption for n_o between 9 and 12. These expectations are in surprisingly good accord with the observations of Christoffel and Bowman [13]. In particular, one could note the increased absorption for $n_o \gtrsim 9$. The fact that a great deal of energy, much more than for the lower n_o values, appears to be absorbed for $n_o \gtrsim 9$ is indicative of the higher order resonances $(n_2, n_3, \ldots)$ being more closely spaced and overlapping to a large extent, allowing the molecule to essentially travel up a "chaotic ladder" of separatrix layers.

This sort of analysis is entirely qualitative, but does have the advantage that an essentially "back of the envelope" calculation yields qualitatively correct predictions of energy absorption trends. Recently, Davis and Wyatt[14] have developed a Poincaré surface of section

approach, based on the numerical integration of only a few classical trajectories, that is complementary to the approach here.

VI. Concluding Remarks

A method of generating period advance maps[3] for one-dimensional forced oscillator problems has been given. An application to a forced Morse oscillator demonstrated that a good deal of dynamical information could be obtained from the approach. The applicability is limited, however, to a relatively modest number ($\lesssim 400$) of map iterations (oscillations of the field), but this can be improved somewhat by increasing the initial grid size. Also, if one is only interested in particular dynamical features, such as the fate of a specific initial classical state, it is of course easier to use direct classical trajectories.

The behavior of the nonrotating HF molecule in a strong laser was found to be quite interesting, with classical states developing whorls[4] in the vicinity of the stable fixed point of the map. In fact, the entire phase plane was seen to consist of whorls of excitation and de-excitation. The pendulum model[5] of nonlinear resonance seems quite applicable to problems of this sort and does reproduce some of the major qualitative features. Also, certain dynamical trends, such as the average energy absorption as a function of initial vibrational state, can be qualitatively discussed with this model. Since the pendulum model has been used[5,15] to treat systems with more than 1 or 2 degrees of freedom, there may be some hope in using similar ideas to interpret the behavior of, say, vibrating and rotating diatomic

molecules in lasers, or more general polyatomics, or perhaps two or more lasers[16] interacting with a molecule. Indeed, in related work, Oxtoby and Rice[15] have treated the autonomous problem of energy re-distribution in polyatomic molecules after excitation using the pendulum model and Chirikov's resonance overlap ideas for the onset of chaotic motion.

As a final point, the quantum analogue of the classical whorls has not been discussed here. Berry and co-workers[4] have discussed this point, and do expect to see certain evidence of whorls in the behavior of the time-dependent probability density.

Acknowledgements

It is a pleasure to acknowledge the support and encouragement of Professor William H. Miller. The comments of Peter S. Dardi were also important for the successful completion of this work. I would also like to acknowledge some very helpful discussions with Professor Robert E. Wyatt, Professor M. A. Lieberman and Dr. Yitzhak Weissman. This work was supported by the Director, Office of Energy Research, Office of Basic Energy Sciences, Chemical Sciences Division of the U. S. Department of Energy, under Contract No.DE-AC03-76SF00098, and also in part by the National Science Foundation under Grant CHE-79-20181. Financial assistance from the NSERC of Canada is also gratefully acknowledged.

Appendix . Fixed Points of the Period Advance Map

An approximate, but surprisingly accurate estimate of the period 1 fixed points is as follows. Starting from eq. (4.6) of the text,

$$K = H_o(\hat{p} + n_1) - \varepsilon V_1(\hat{p} + n_1)\ \cos\hat{q} - \hat{p}\Omega \quad , \qquad \text{A1}$$

where $\hat{q} = q - \Omega t$ and $\hat{p} = n - n_1$, one then uses the harmonic oscillator[11,17] $x(n,q)$ to estimate V_1, rather than the exact form eq. (4.3b). This is valid for small n and simplifies the calculations. Thus

$$\begin{aligned} V_1(n) &= (2\pi)^{-1} \int_{-\pi}^{\pi} x(n,q)\ \cos q\ dq \\ &= (2\pi)^{-1} \int_{-\pi}^{\pi} \sqrt{(2n+1)/\mu\omega_o}\ \cos^2 q\ dq \\ &= \sqrt{(2n+1)/\mu\omega_o}\ /2 \quad . \end{aligned} \qquad \text{A2}$$

Eq. A1 becomes

$$K = H_o(\hat{p} + n_1) - (\varepsilon/2)\ \sqrt{[\,2(\hat{p} + n_1) + 1\,]/\mu\omega_o}\ \cos\hat{q} - \hat{p}\Omega \quad . \qquad \text{A3}$$

The equations of motion consistent with the Hamiltonian above are

$$\begin{aligned} \dot{\hat{p}} &= -(\varepsilon/2)\ \sqrt{[2(\hat{p} + n_1) + 1]/\mu\omega_o}\ \sin\hat{q} \\ \dot{\hat{q}} &= \omega(\hat{p}+n_1) - \frac{(\varepsilon/2)\ \cos\hat{q}}{\sqrt{\mu\omega_o\ [2(\hat{p} + n_1) + 1]}} - \Omega \quad . \end{aligned} \qquad \text{A4}$$

For a fixed point, we require $\dot{\hat{p}} = \dot{\hat{q}} = 0$. Replacing $\hat{p} + n_1$ by n, and setting t = 0 so that $\hat{q} = q$, we obtain the two equations

$$-(\varepsilon/2)\sqrt{(2n+1)/\mu\omega_o}\,\sin q = 0 \qquad \text{A5a}$$

$$\omega(n) - \frac{(\varepsilon/2)\cos q}{\sqrt{\mu\omega_o(2n+1)}} - \Omega = 0 \ . \qquad \text{A5b}$$

Eq. A5a is satisfied for q = 0 and π. Inserting either of these into eq. A5b yields a simple one-dimensional root equation for n, which can be solved by iteration. With the parameters of sec. IIIB, one finds the fixed points (n,q) = (0.6218, π), (0.3610, 0), and (-0.4828, 0), which are in remarkably good agreement with the more exact fixed points, which were found to be (0.6173, π), (0.3603, 0), and (-0.4821, 0). An even more accurate estimate of the fixed points could be obtained by using eq. (4.3b) for V_1.

References

1. See, for example, "Advances in Laser Chemistry", ed. A.H. Zewail, (Springer, New York, 1978) and "Laser-Induced Processes in Molecules", ed. K.L. Kompa and S.D. Smith, (Springer, New York, 1978).

2. (a) R.B. Walker and R.K. Preston, J. Chem. Phys. 67 (1977) 2017.
(b) D.C. Noid, C. Bottcher, and K.L. Koszykowski, Chem. Phys. Letters 72 (1980) 397.
(c) P.S. Dardi and S.K. Gray, J. Chem. Phys., to be published.

3. (a) V.I. Arnold and A. Avez, "Ergodic Problems in Classical Mechanics", (Springer, New York, 1968) p. 83.
(b) V.I. Arnold, "Mathematical Methods of Classical Mechanics", (Springer, New York, 1978) p. 114.

4. M.V. Berry, N.L. Balazs, M. Tabor, and A. Voros, Annals Phys. 122 (1979) 26.

5. (a) B.V. Chirikov, Phys. Rep. 52 (1979) 263.
(b) G.M. Zaslavskii and B.V. Chirikov, Sov. Phys. Usp. 14 (1972) 549.

6. See, for example, H.T. Davis, "Introduction to Nonlinear Differential and Integral Equations", (Dover, New York, 1962).

7. (a) S.C. Leasure and R.E. Wyatt, Opt. Eng. 19 (1980) 46.
(b) S.C. Leasure, K.F. Milfeld, and R.E. Wyatt, J. Chem. Phys. 74 (1981) 6197.

8. (a) L.F. Shampine and R.C. Allen, "Numerical Computing: an Introduction", (Saunders, Philadelphia, 1973).
(b) D.R. McLaughlin and D.L. Thompson, J. Chem. Phys. 59 (1973) 4393; see also N. Sathyamurthy and L.M. Raff, J. Chem. Phys. 63 (1975) 464.

9. C.C. Rankin and W.H. Miller, J. Chem. Phys. 55 (1971) 3150. Note that their phase convention for q differs by π from ours and their energy is with respect to the separated atoms as zero.

10. See, for example, M.V. Berry, in: "Topics in Nonlinear Dynamics", ed. S. Jorna, (AIP, New York, 1978) Chapter 2.

11. H. Goldstein, "Classical Mechanics", (Addison-Wesley, Reading, MA, 1950).

12. I.S. Gradshteyn and I.M. Ryzhik, "Table of Integrals, Series, and Products", (Academic, New York, 1965). See, e.g., formula 4.398.

13. K.M. Christoffel and J.M. Bowman, J. Phys. Chem. 85 (1981) 2159.

14. M.J. Davis and R.E Wyatt, Chem. Phys. Letters 86 (1982) 235.

15. D.W. Oxtoby and S.A. Rice, J. Chem. Phys. 65 (1976) 1676.

16. R.J. Stine and D.W. Noid, Opt. Commun. 31 (1979) 161.

17. W.H. Miller, J. Chem. Phys. 53 (1970) 3578.

Table I. Root mean square deviations between the map predictions and direct numerical integration of trajectories. The results are for 50 trajectories with $n_o = 0$ initially. Typical values of p and x are ± 3 and 2 a.u. respectively.

	R.M.S. deviation	
r	p	x
100	0.005	0.0001
200	0.008	0.0003
300	0.016	0.0010
400	0.024	0.0020
500	0.078	0.0029

Figure Captions

Figure 1. Surface of section plots of the period advance map. a) p-x space, b) n-q space. Open circles (o) represent stable fixed points and filled circles (•) unstable fixed points. Note the arrows do not imply a continuous flow. Rather, points take discrete and uneven jumps to other points on the same curve, in the direction indicated.

Figure 2. The evolution of an initial $n_o = 1/2$ state under the mapping. a) the result after r = 20 periods. Note the dashed line represents the initial state. b) after 40 periods, c) after 60 periods.

Figure 3. a) the result of mapping an $n_o = 0$ state 40 periods, b) the result of mapping an $n_o = 1$ state 40 periods. Dashed lines indicate the initial states.

Figure 4. Evolution of the entire n-q phase plane. a) after 20 periods, b) after 40 periods, c) after 60 periods. The contours represent a coarse grained action state. See the text for more details.

Figure 5. The pendulum model predictions for the fate of initial states a) $n_o = 1/2$, b) $n_o = 0$, and c) $n_o = 1$, after 40 periods.

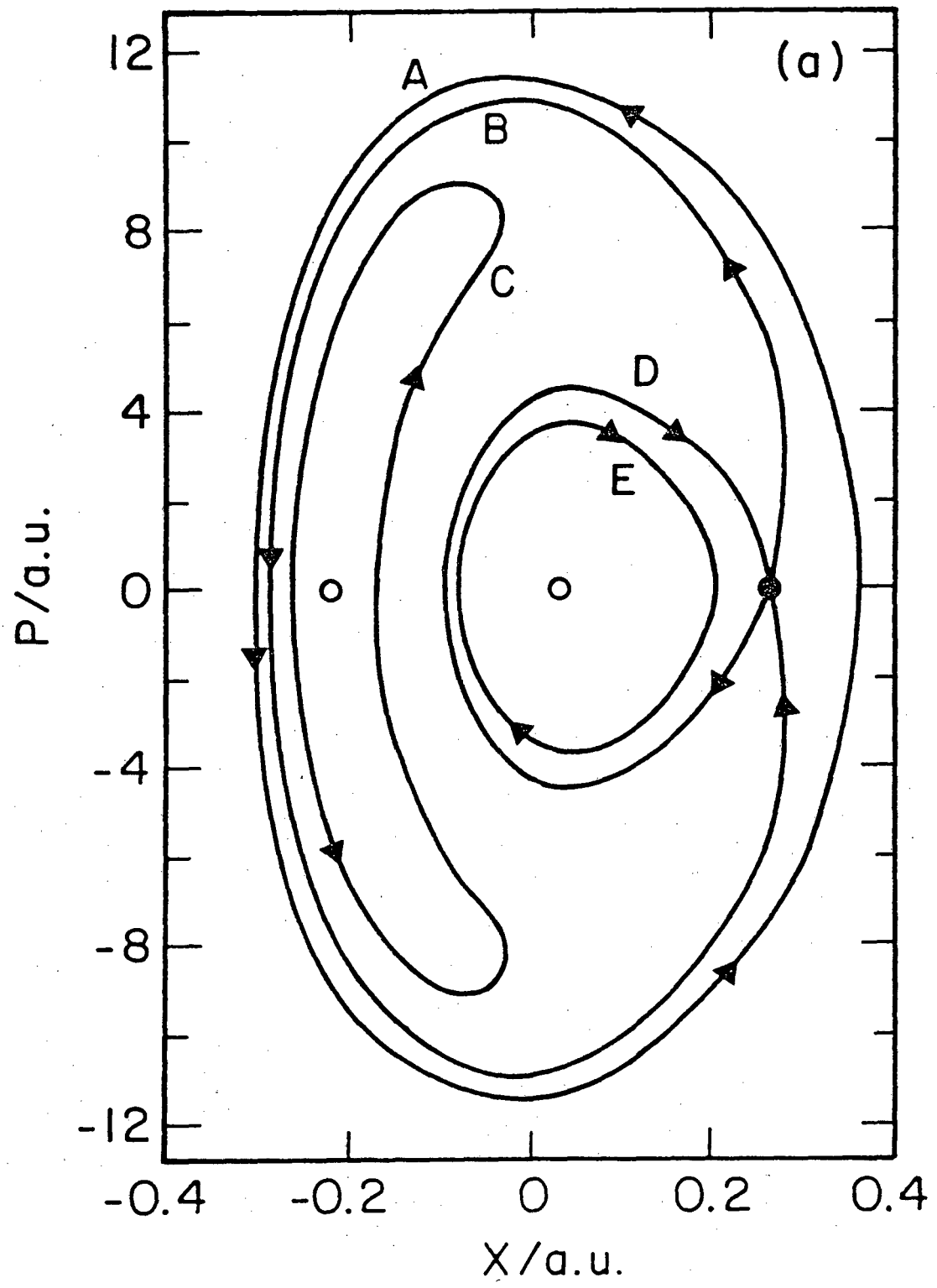

Figure 1a.

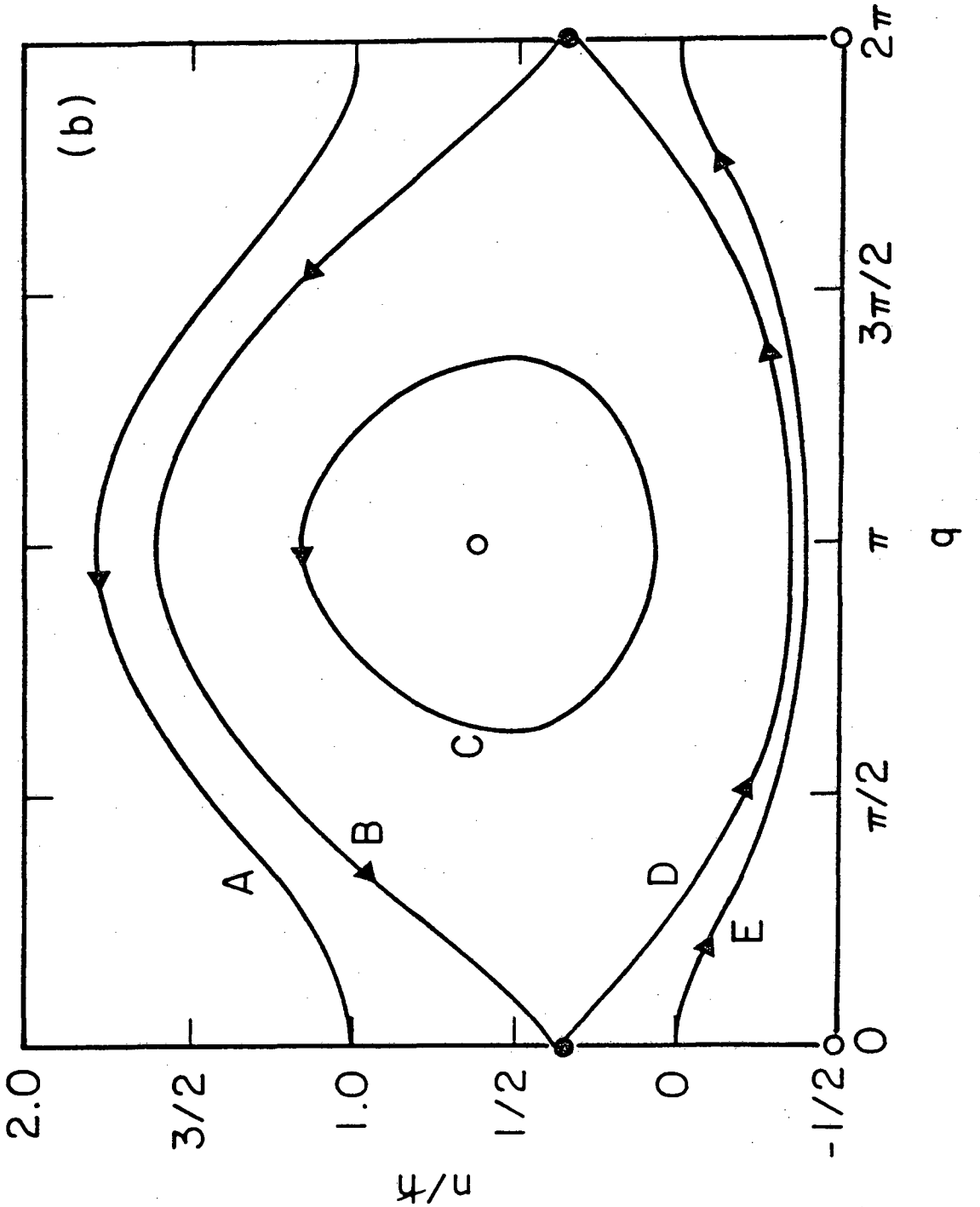

Figure 1b.

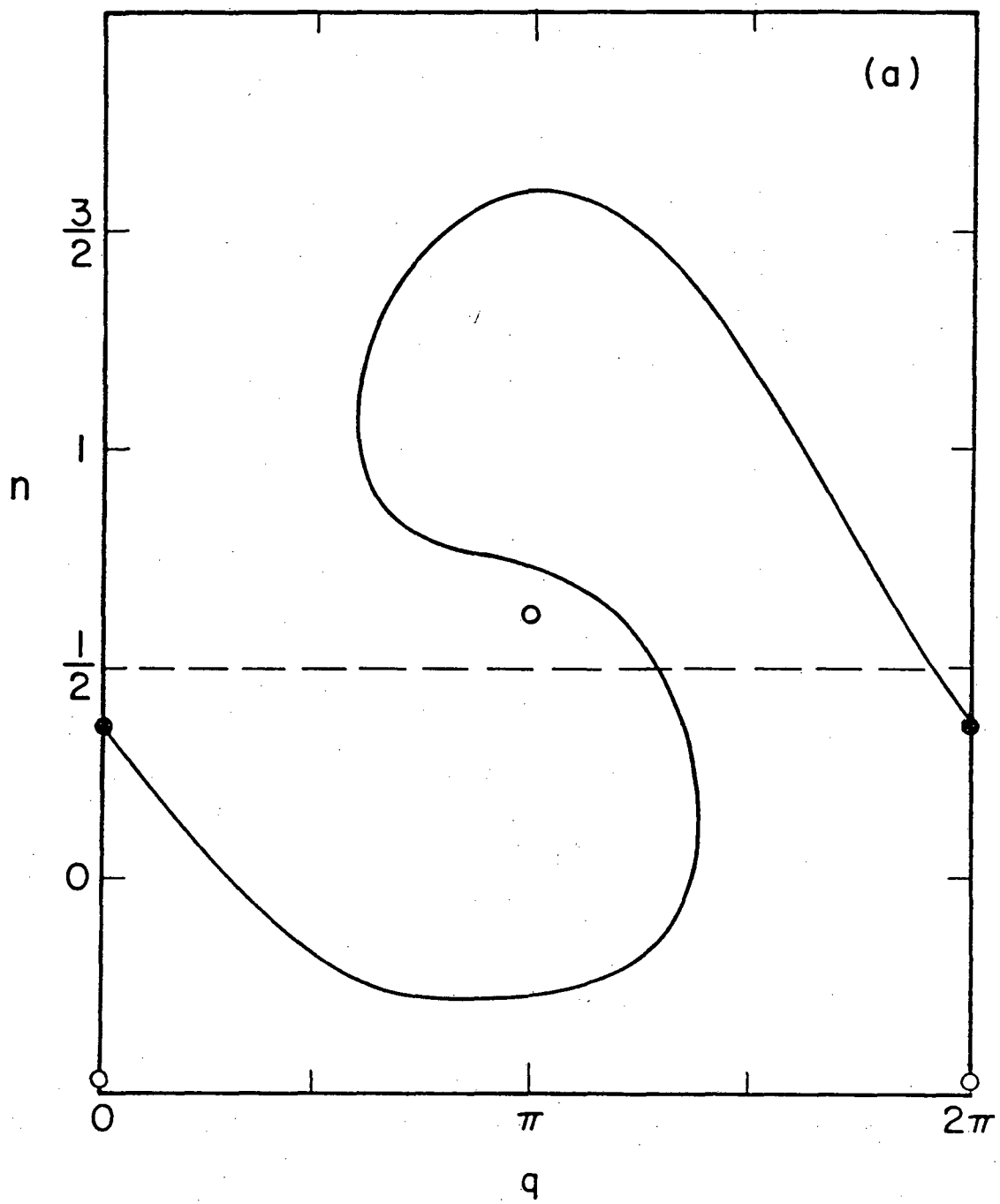

Figure 2a.

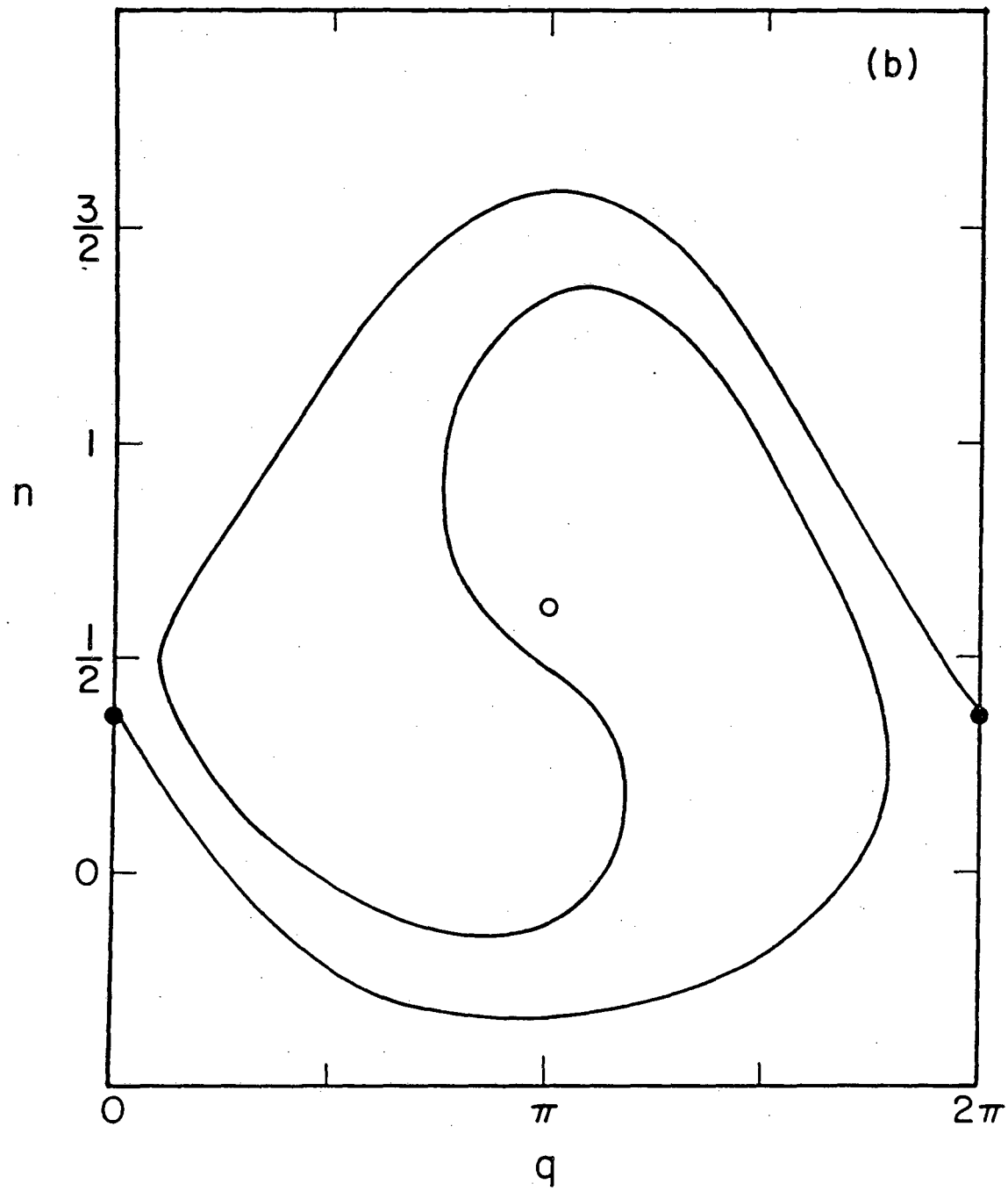

Figure 2b.

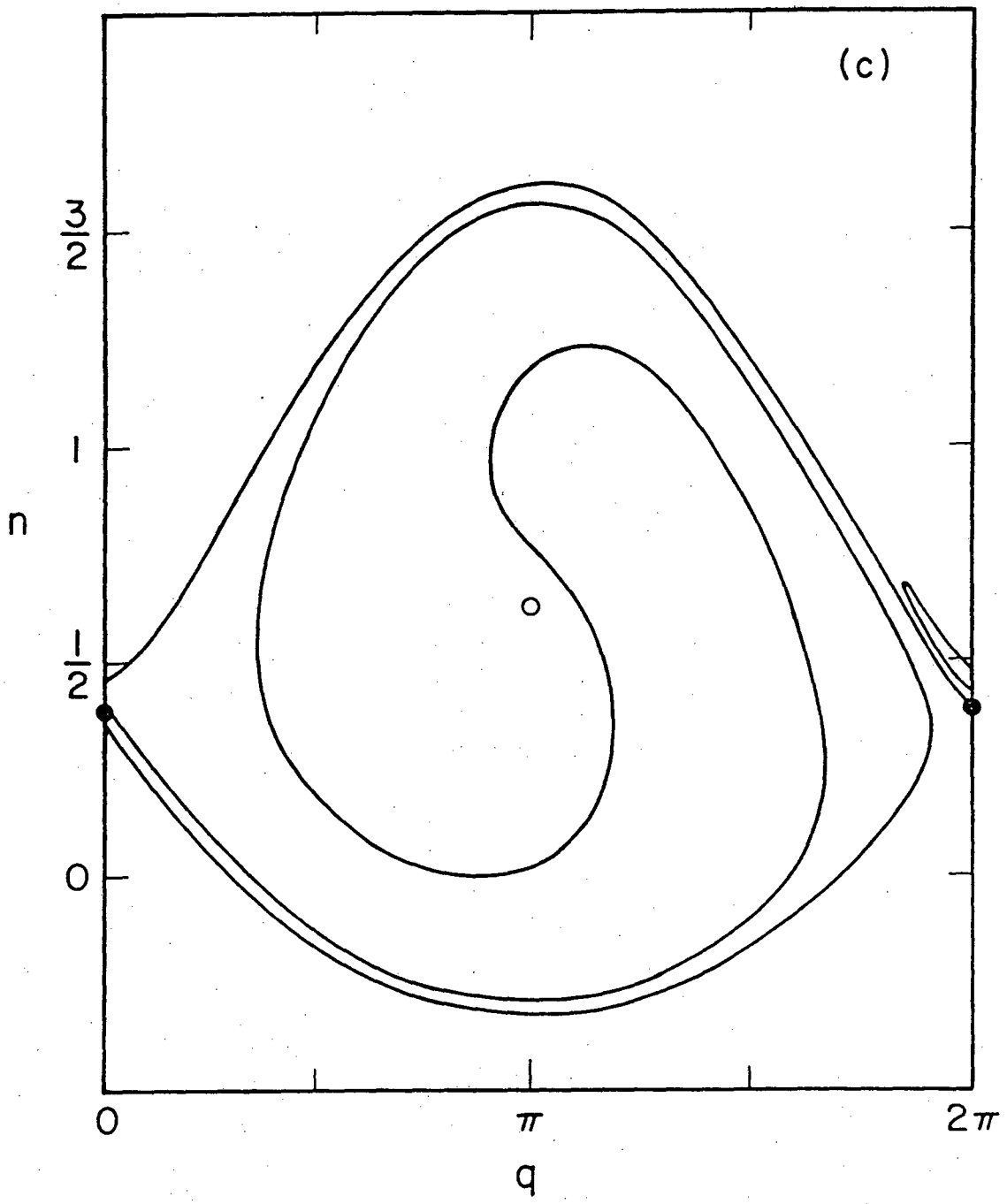

Figure 2c.

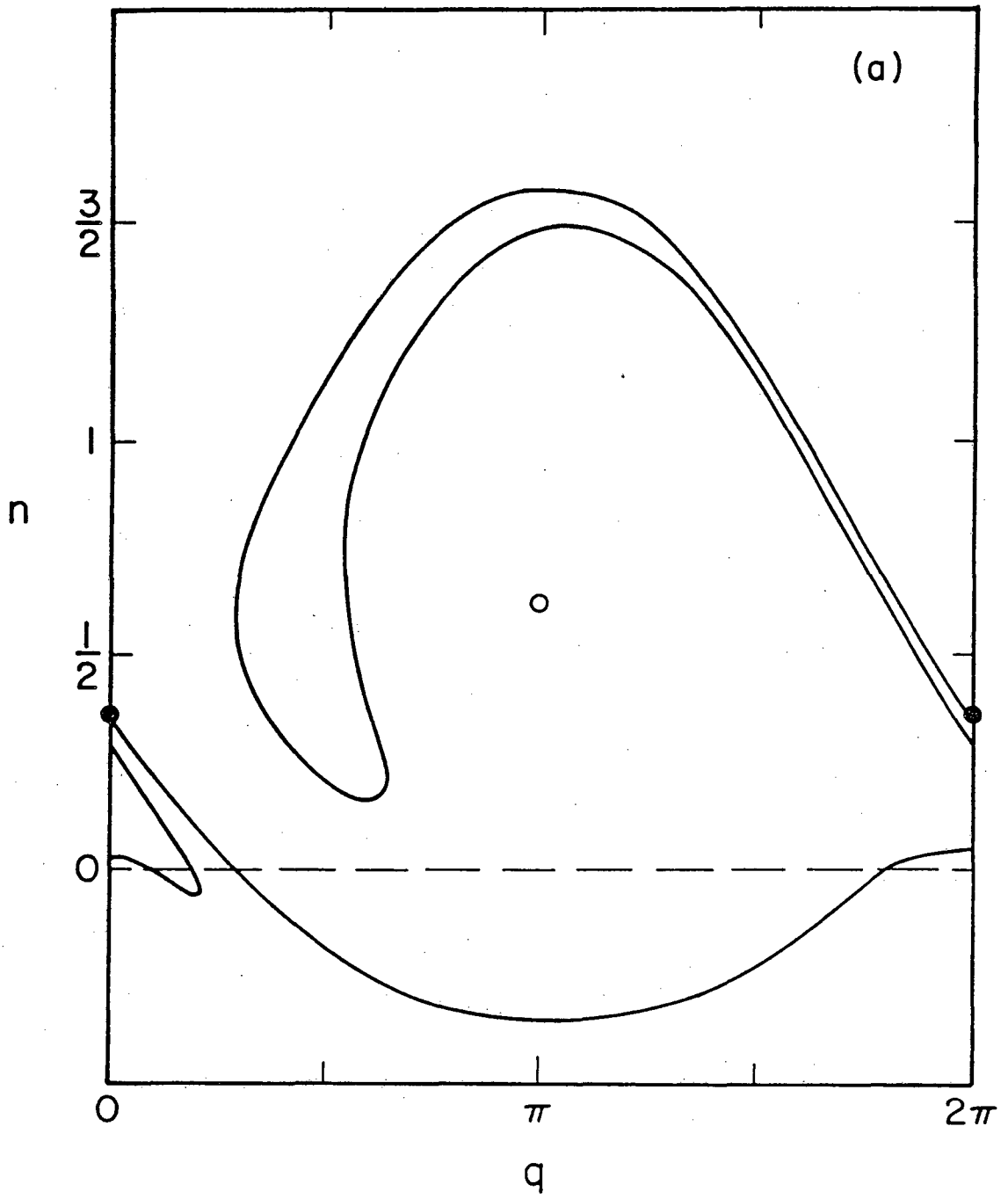

Figure 3a.

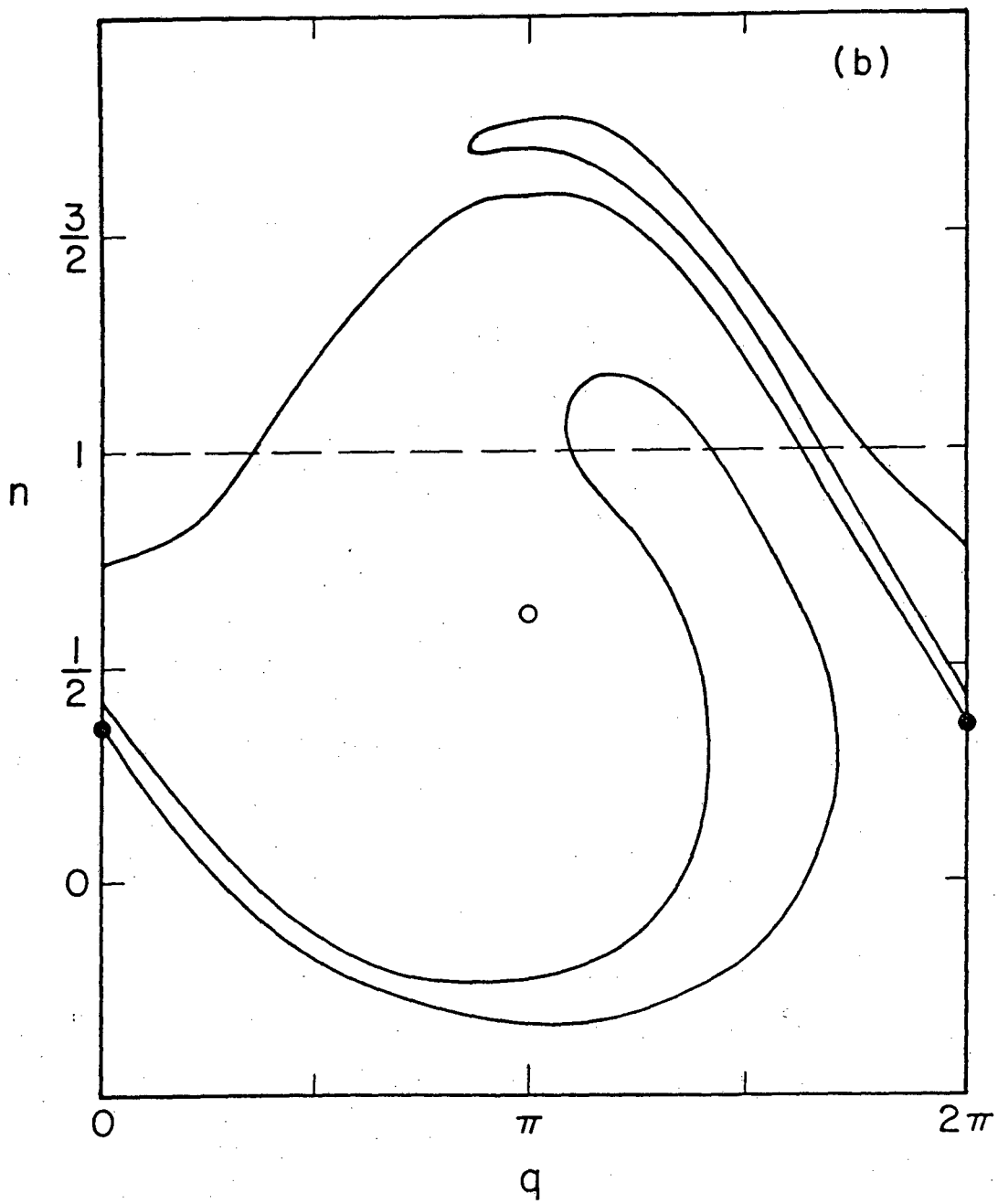

Figure 3b.

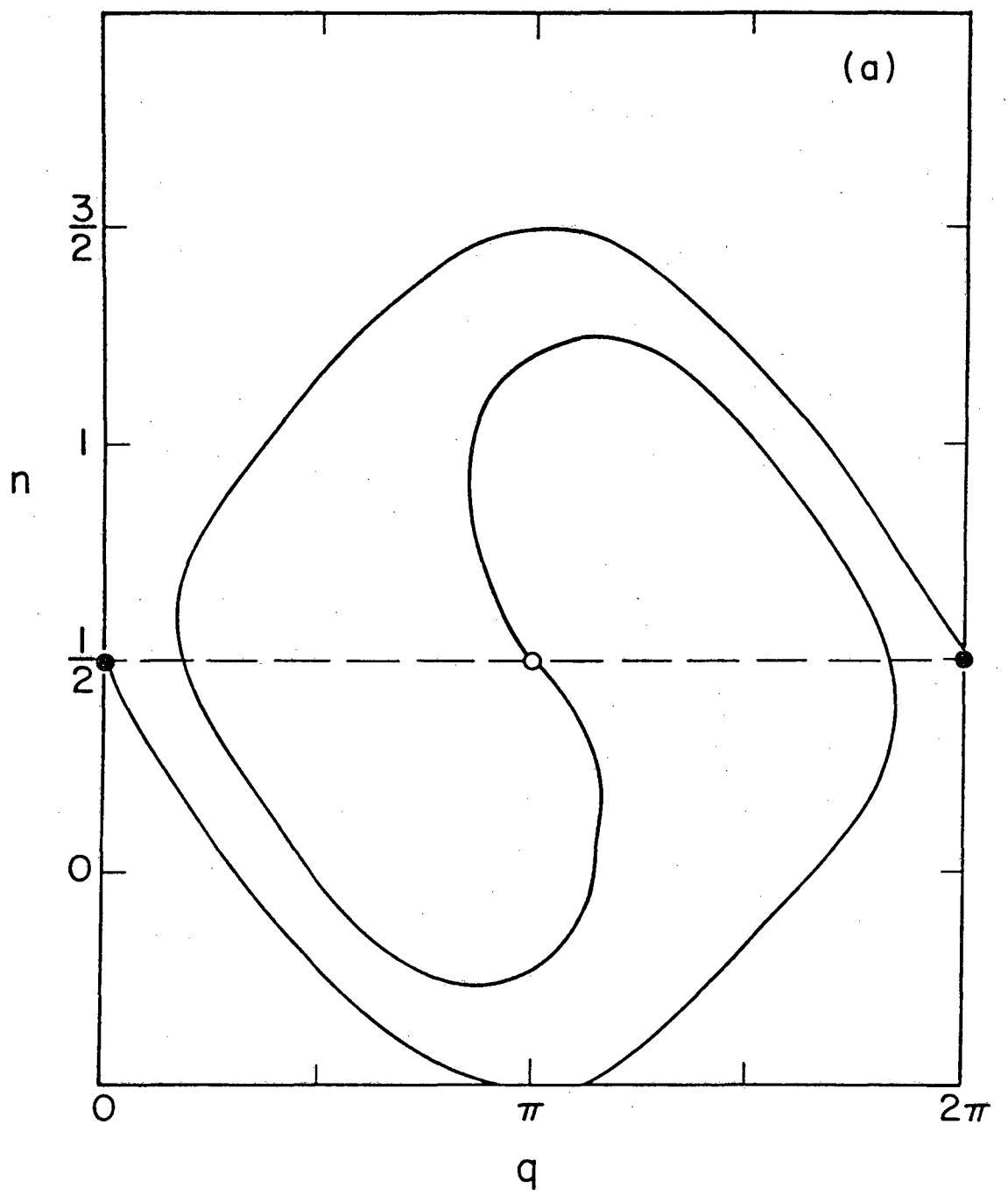

Figure 4a.

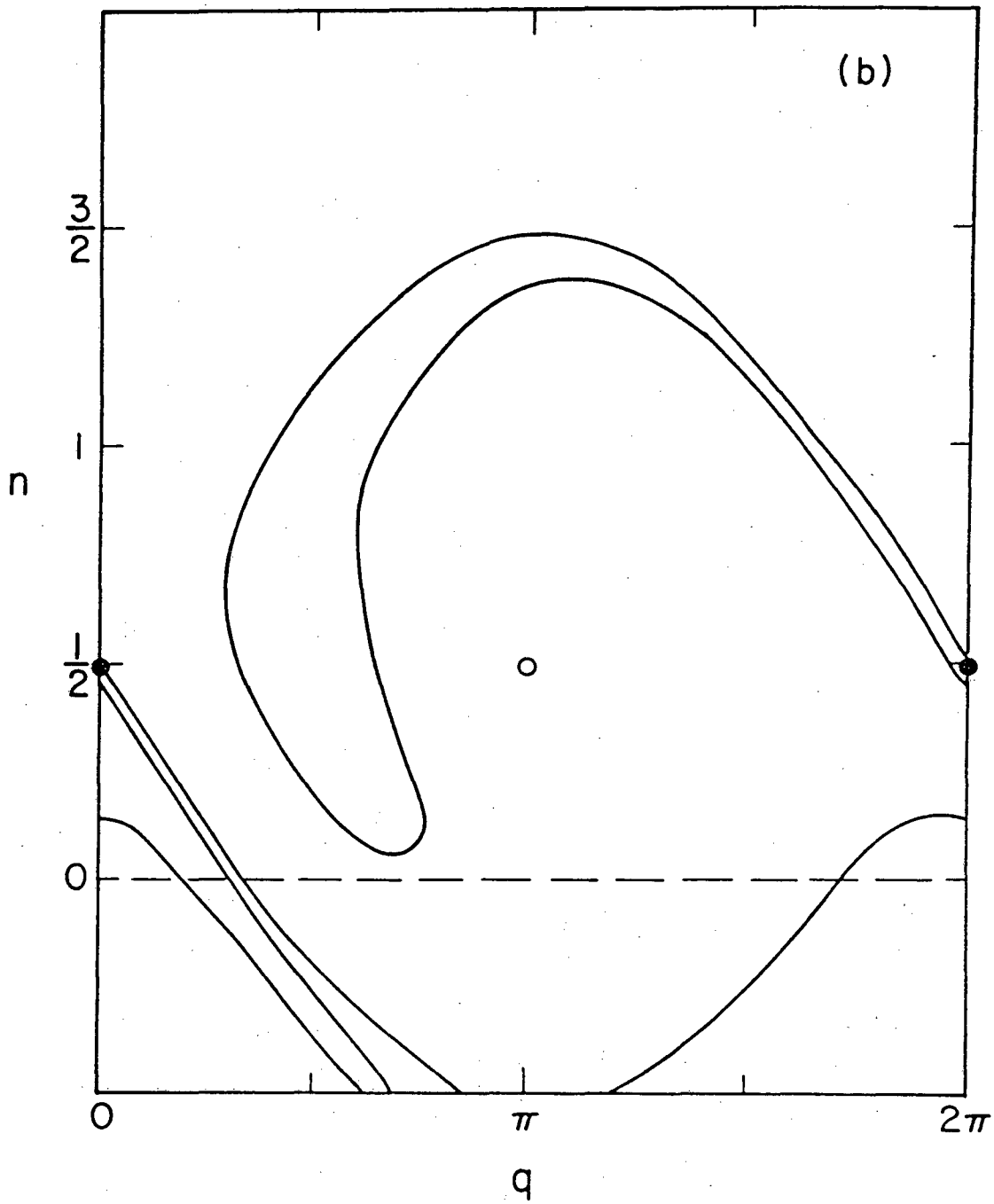

Figure 4b.

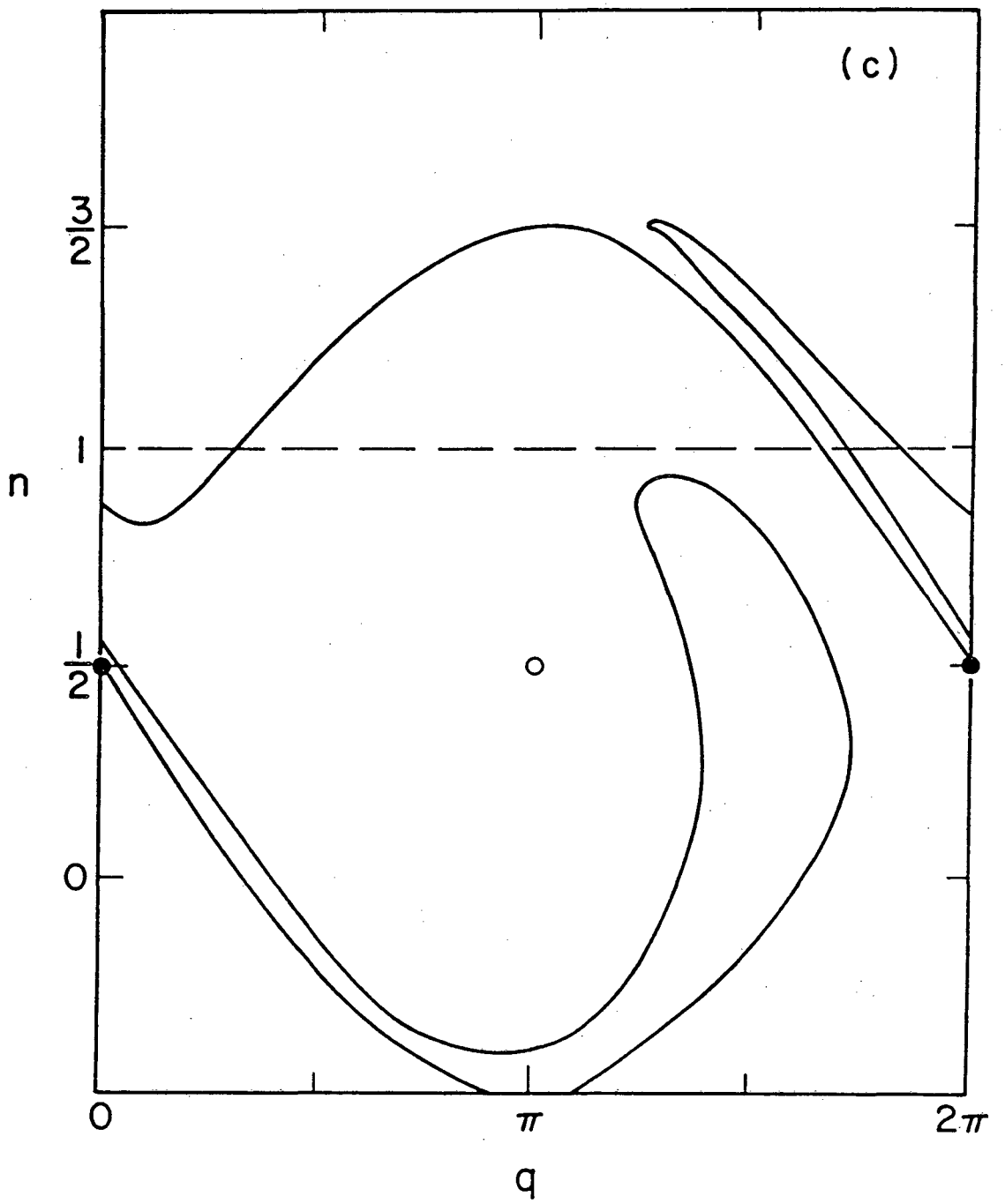

Figure 4c.

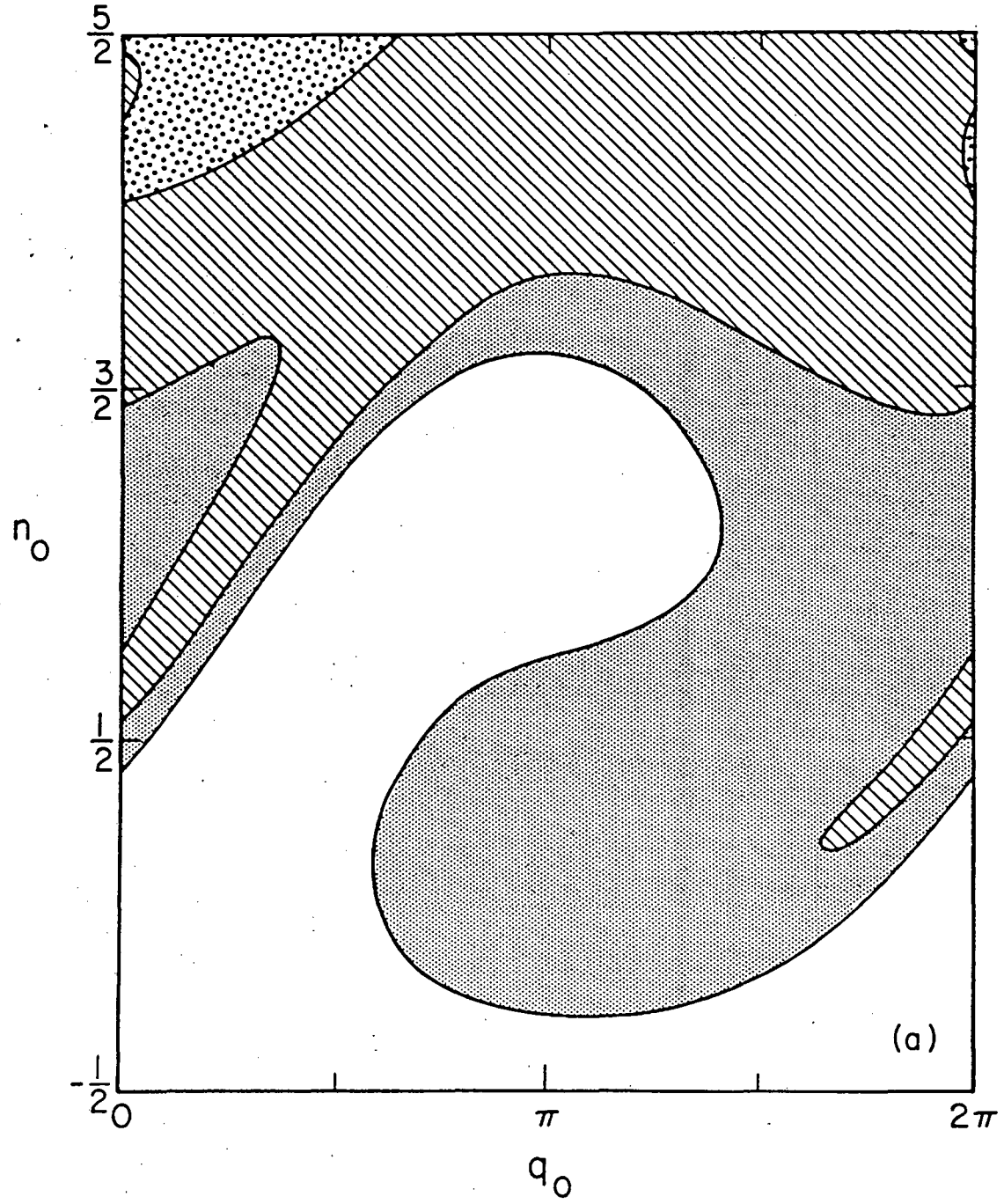

Figure 5a.

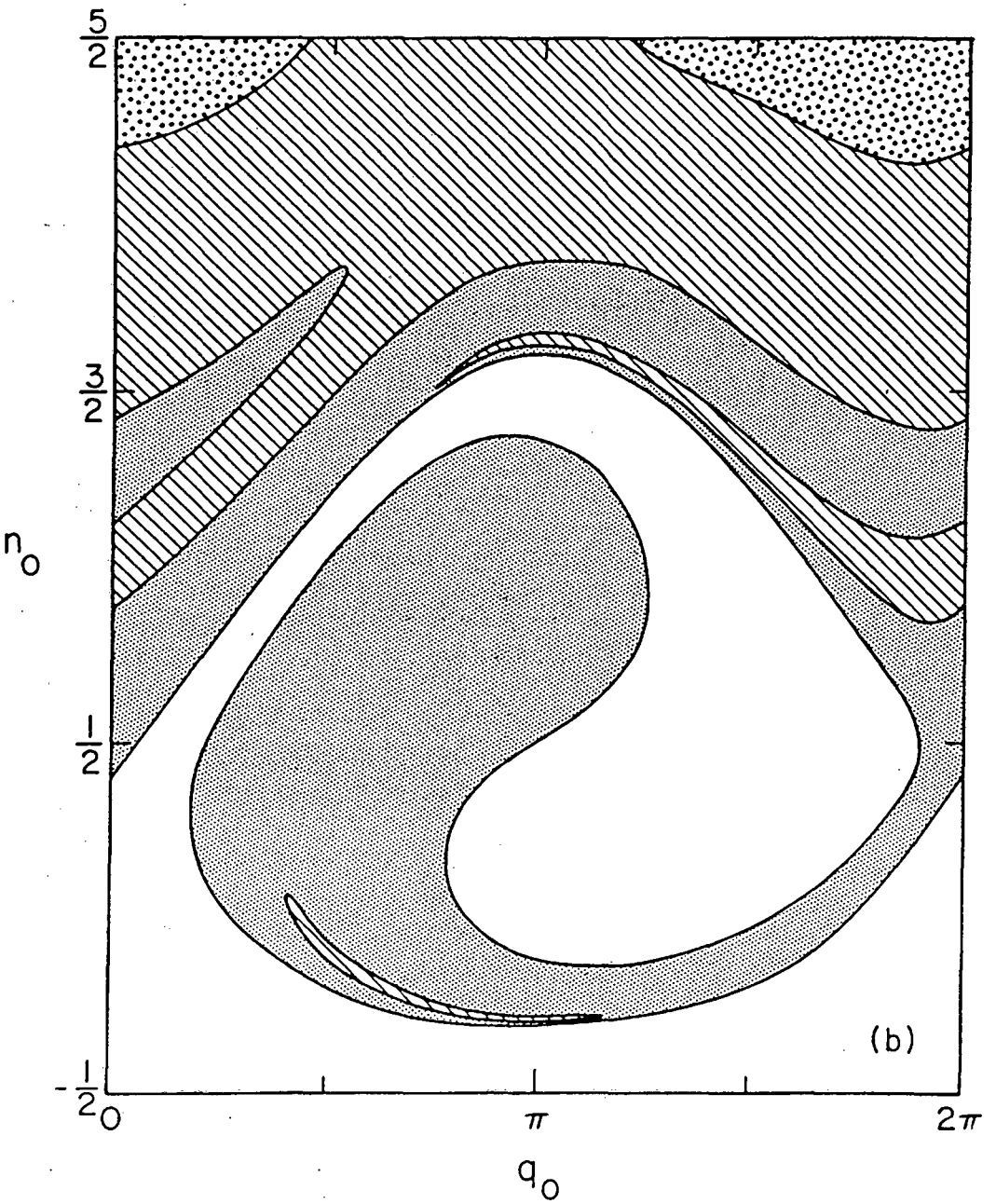

Figure 5b.

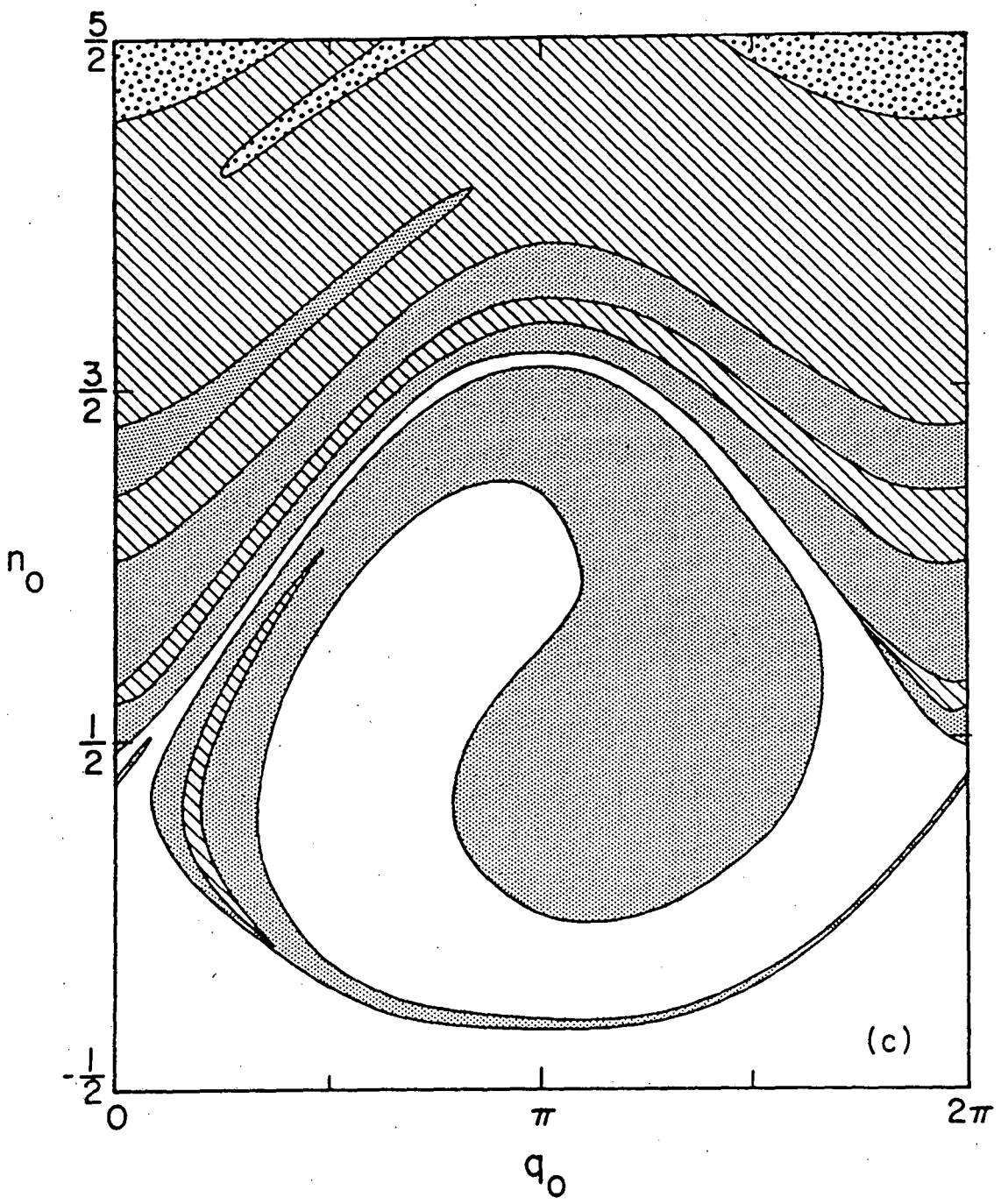

Figure 5c.

TECHNICAL INFORMATION DEPARTMENT
LAWRENCE BERKELEY LABORATORY
UNIVERSITY OF CALIFORNIA
BERKELEY, CALIFORNIA 94720